International Journal of Pharmacy and Pharmaceutical Sciences
ISSN- 0975-1491 Vol 2, Suppl 3, 2010

Research Article

QSAR MODELING AND PHARMACOPHORE MAPPING OF ISOFLAVONE DERIVATIVES FOR AROMATASE INHIBITORY ACTIVITY♣

SHUCHI NAGAR, ACHINTYA SAHA*

Department of Chemical Technology, University of Calcutta, 92, A.P.C. Road, Kolkata-700009 (India) ♣Presented in International Conference on Biochemistry and Medical Chemistry (BIOMEDCH'10), University of Cambridge, UK, February 23-25, 2010, Email: achintya_saha@yahoo.com

Received: 18 April 2010, Revised and Accepted: 01 May 2010

ABSTRACT

The key role of aromatase in estrogen biosynthesis has generated enormous interest in putative inhibitors of the enzyme and their use as therapy against endocrine responsive tumors. In view of significance, QSAR modeling and pharmacophore mapping have been explored to investigate the structural requirement of isoflavone (Fig 1) derivative for inhibition of aromatase (CYP19) enzyme. The best model generated in classical QSAR study (R^2=0.895, Q^2=0.726, R^2_{pred} =0.780) shows that substitutions by electron withdrawing group at atom C_{14} and electron rich group at O_{18} are important for promoting the activity. Further molecular ionization potential and steric factors also influence the inhibitory activity to CYP19. 3D QSAR study of molecular field analysis (R^2=0.996, Q^2=0.841, R^2_{pred}=0.936) shows the importance of steric and electrostatic fields for the inhibitory activity. Similarly, molecular similarity analysis (R^2=0.997, Q^2=0.802, R^2_{pred}=0.899) signifies the importance of hydrogen bond acceptor and hydrophobic features in addition to steric and electrostatic force fields that play role in inhibiting the enzyme. Pharmacophore mapping (Q^2=0.859, Δ_{cost}=105.597, R^2_{pred}=0.912) study adjudges the significance of hydrogen bond acceptor and hydrophobic features of the molecule, and 3D distances among features are critical for the inhibitor activity.

Keywords: QSAR; CoMFA; CoMSIA; Pharmacophore; Isoflavone; Aromatase Inhibitor.

INTRODUCTION

Breast cancer is the second leading cause of cancer death in women in the United States. About 180,000 women in the United States are found to have invasive breast cancer in 2007[1]. The role of endogenous estrogen in the development of breast cancer has long been recognized[2] and estrogens are known to play pivotal role in the proliferation of cancer cells[3]. Aromatase enzyme[4] catalyzes the rate limiting step in estrogen biosynthesis[5]. On aromatization of A-ring of androgen to form the phenolic A-ring (characteristic feature) of estrogen with concomitant loss of 19-angular methyl group[6,7,8]. Thus inhibition of aromatase enzyme is an attractive target for the endocrine treatment of hormone dependent breast cancer[9]. Some third generation aromatase inhibitors (AIs), exemestane, letrozole are presently in use for breast cancer treatment. On the basis of their inhibitory mechanisms, these molecules are divided[10] into two classes: (1) irreversible steroid inactivators such as formestane or exemestane that bind covalently to the enzyme, and (2) non-steroidal inhibitors such as letrozole or anastrozole that act as reversible competitive inhibitors.

Developments in the design of new AIs could be obtained through computer aided drug designing (CADD) techniques. Computational/molecular techniques or chemometric studies can gift us molecules with optimistic efficacy. CADD is categorized into target protein- and small molecule (ligand) – based approach. Process initiation from hits or leads range from pharmacophore or multidimensional quantitative structure activity relationship (QSAR) models and binary scoring to compound clustering and statistical techniques capable of analyzing datasets and deriving predictive models of bioactivity. The importance of all three processes is on resource management and minimization of animal sacrifice.

Molecular modeling studies have been performed on various non-steroidal AIs[11,12,13,14] to explore their pharmacophore. The studies showed the importance of intrinsic molecular hydrophobicity and hydrogen bond acceptors for inhibitory activity. In the present modeling study, isoflavone derivatives[15] (Fig 1) are explored to derive the pharmacophore/structural requirement for inhibiting aromatase activity using quantitative structure activity relationship (QSAR) and space modeling studies. QSAR studies are used to develop statistically validated models that give structural explanation towards activity. The popular 3D QSAR methods, Comparative Molecular Field Analysis (CoMFA)[16,17] and Comparative Molecular Similarity Analysis (CoMSIA)[18,19] involve the generation of a common 3D lattice around a set of molecules. CoMFA accomplishes the calculation of the steric and electrostatic interaction energies at the lattice points, whereas CoMSIA uses similarity functions represented as Gaussian. The information around the molecule are transferred into numerical data using the partial least squares (PLS)[20] method that reduces the dimensionality of data by generating components that can correlate with bioactivity. On the other hand, space modeling study generates a pharmacophore hypothesis[21], which is a set of functional group/fragment types in a spatial arrangement that represent the interaction made in a common scaffold by a set of small molecular ligands with a protein receptor. The pharmacophore concept is based on the kinds of interaction observed in molecular recognition and alternatively can be used as a query in a 3D database search to identify new structural classes of potential lead compounds, and it can serve as a template for generating alignment for 3D QSAR analysis.

MATERIALS AND METHODS

The molecular dataset[15] (Table 1) is randomly divided into training (Tr) and test (Ts) sets for the study. The CYP19[4] inhibitory activity (IC_{50}, μM) has been considered as biological activity and implemented as logarithmic function, pIC_{50} ($\log_{10}1000/IC_{50}$) for modeling purpose. The objective of the work is to generate relationship between structure and corresponding activity through QSAR studies and deduce a pharmacophore map through receptor-independent space modeling technique[21]. Multiple linear regression (MLR)[22] and PLS[20] techniques are applied for QSAR studies.

QSAR Study

3D structure of molecules are minimized in MOPAC using AM1 method to locate their global minima conformers and subsequent calculation of different molecular properties, such as physiochemical, electronic, topological, and spatial and structural features are estimated for classical modeling[23]. The partial charge is calculated using the Extended Huckel approach[24], and *E*-state index[25] of all the atoms (Fig 1) are generated using a JAVA-based program[26], while other descriptors are generated using Chem3D Pro[24], CAChe[27] and TSAR[28]. MLR is performed using standard and forward stepwise regression techniques[22].

Table 1: Structural features and inhibitory activity of Isoflavone derivatives

Compd no	R_1	R_2	R_3	IC_{50} (μM)	pIC_{50}
1	H	Benzyl	4′-Pyridyl-thio	0.210	3.678
2	H	2′-Nitrophenylmethyl	4′-Pyridyl-thio	0.138	3.860
3*#	H	3′-Nitrophenylmethyl	4′-Pyridyl-thio	0.113	3.947
4	H	4′-Nitrophenylmethyl	4′-Pyridyl-thio	0.132	3.879
5	H	α-Naphthylmethyl	4′-Pyridyl-thio	0.112	3.951
6	H	β-Naphthylmethyl	4′-Pyridyl-thio	0.090	4.046
7*#	H	Benzyl	4′-Pyridyl-thio	0.359	3.445
8	H	2′-Methoxy-phenylmethyl	4′-Pyridyl-thio	0.243	3.614
9	H	4′-Methoxy-phenylmethyl	4′-Pyridyl-thio	0.161	3.793
10	H	Cyclohexylmethyl	4′-Pyridyl-thio	0.553	3.257
11	H	4′-Flurophenylmethyl	4′-Pyridyl-thio	0.337	3.472
12#	H	4′-Bromophenylmethyl	4′-Pyridyl-thio	0.213	3.672
13	H	4′-Chlorophenylmethyl	4′-Pyridyl-thio	0.233	3.633
14	H	4′Biphenylmethyl	4′-Pyridyl-thio	0.079	4.102
15	H	2′-Pyridylmethyl	4′-Pyridyl-thio	0.378	3.423
16*	H	Methyl	Imidazol-1-yl	0.770	3.114
17	OMe	Methyl	Imidazol-1-yl	2.000	2.699
18	H	Benzyl	Imidazol-1-yl	0.520	3.284
19	H	Methyl	1H—1,2,4-triazol-1-yl	18.000	1.745
20*#	H	Methyl	(4′-pyridyl)methyl-thio	1.600	2.796
21	H	Methyl	(3′-pyridyl)methyl-thio	9.200	2.036
22	H	Methyl	(2′-pyridyl)methyl-thio	3.000	2.523
23#	Me	Methyl	(4′-pyridyl)methyl-thio	3.100	2.509
24	H	OH	(4′-pyridyl)methyl-thio	0.610	3.215
25	H	OH	(4′-pyridyl)methy-thio	3.600	2.444
26	OH	OH	(4′-pyridyl)methyl-thio	0.280	3.553
27	OMe	OH	(4′-pyridyl)methyl-thio	0.220	3.658

*Ts set compounds for QSAR studies

#Ts set for compounds pharmacophore study

QSAR model origination is accomplished by correlation analysis using Statistica[29], and the statistical parameters of the regression equation considered are R^2 (correlation coefficient), *EV* (explained variance), *F* (variance ratio), *df* (degree of freedom), *se* (standard error of estimate), and *AVRES* (average of absolute values of calculated residuals). Leave-one-out (LOO) cross-validation[30] is performed to obtain Q^2 (cross-validated variance).

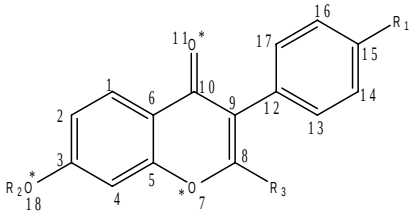

Fig. 1: General structure of isoflavone molecular scaffold with atoms considered for alignment are marked as *

3D-QSARs, CoMFA and CoMSIA models permit an understanding of steric (s) and electrostatic (e)[31], lipophilic/hydrophobic (p)[32], and hydrogen bond (HB) acceptor (a) and donor (d) requirements for ligand functionality. The structural variation in the Tr set that gives rise to variation in the molecular fields at particular regions of the space are correlated to the biological property. In both cases conformers are generated by simulated annealing technique[33]. The molecules are heated at 700 K for 1000 fs and annealing is done at 200 K for 1000 fs. Partial atomic charges are calculated by the Gasteiger-Huckel method[34] and energy minimization are performed using the Tripos force field[35,36]. Both CoMFA and CoMSIA studies provide presentable models when database alignment of molecular conformer is done on a template. In the present study, the most active compound (IC_{50}=0.079 μM) is selected as template and points are defined as shown in Fig 1. PLS approach[20] is used to derive the 3D QSAR models in which field and similarity factors are the independent variables and inhibitory activity (pIC_{50}) being the dependent variable.

Pharmacophore space modeling study

Pharmacophore mapping of isoflavone derivatives as AI is accomplished by Catalyst[37]. The chemical features optimized for exploring this spatial pharmacophore map[21] of this group of compounds are HB 'a' and 'd', 'p', and ring aromatic (r). The different control parameters employed for hypothesis generation (hypogen process) are uncertainty and weight variation, and each feature signifies some degree of magnitude of the compound's activity. The hypothesis also estimates the cost of null and fixed hypotheses. The greater the difference between the fixed and the null costs, it is more likely that the hypothesis does not reflect a chance correlation. Further the closer the value of total cost to the fixed cost, better the hypothesis as it is more towards the ideal hypothesis. The minimum difference between the total and null costs is taken as 60 bits for a hypothesis optimization[38]. The quality of hypothesis is further adjudged through a cross-validation technique using CatScramble based on Fischer's randomization test[22], where the biological activity data are randomized within a fixed chemical data set and the hypogen process is initiated. By logic, the hypothesis generated prior to scrambling should be better to attest for a good pharmacophore model.

RESULTS AND DISCUSSION

QSAR study

Classical QSAR modeling of isoflavone derivatives (Fig 1) for CYP19 aromatase inhibition has derived the best single variate model with shape factor (Kappa index)[39] that can explain 65.5% variance in activity, and the statistical quality of the relation is estimated to be

R^2= 0.671, *se*= 0.387, *n*=23

And in the case of a bivariate relationship, the best significant relationship has been explored with the same shape factor and e-state index[24] of atom O_{18}, that explained 83.7% variance in activity. The quality of this relationship has been estimated to be

R^2= 0.852, *se*= 0.266, *n*=23

But, the best linear QSAR model of isoflavone derivatives for CYP19 inhibition has been deduced to be

$$pIC_{50} = 0.871\ (\pm 0.336)IP + 0.039(\pm 0.003)MR - 0.853(\pm 0.261)S_{14} + 0.119(\pm 0.027)S_{18} - 8.708(\pm 3.084)$$

Model [1]

Where, *IP* is ionization potential[40], *MR* is molar refractivity[41], S_{14} and S_{18} are e-state indices[24] of atoms C_{14} and O_{18} (Fig 1) respectively. The independent variables used in the model are not inter-correlated (R < 0.5). The statistical quality of the model is

n=23; R^2=0.895; *EV*=87.10%; *F*=38.180; *df*=4,18; *se*=0.237; *AVRES*=0.173; *PRESS*=2.655; Q^2=0.726; R^2_{pred} = 0.780 (Ts set).

The model is accounted for more than 87% variance in observed activity with cross-validated variance (CVV)[29] of 72%. The observed vs predicted activity as per model (1) is depicted in Fig 2.

The model deduced that ionization potential has a positive contribution, suggesting that molecular substitutions that lead to increase in ionization potential of the molecule may favor the activity. Further the positive contribution of MR indicates that steric property of the molecule is favorable for the activity. The negative contribution of S_{14} indicates that low e- density at position C_{14} is favorable, whereas positive contribution of S_{18} denotes that high electron density at position O_{18} favors the activity. Thus electron withdrawing substituent at C_{14}, and group/substitutent that imparts more electron density at O_{18} increase inhibitory activity.

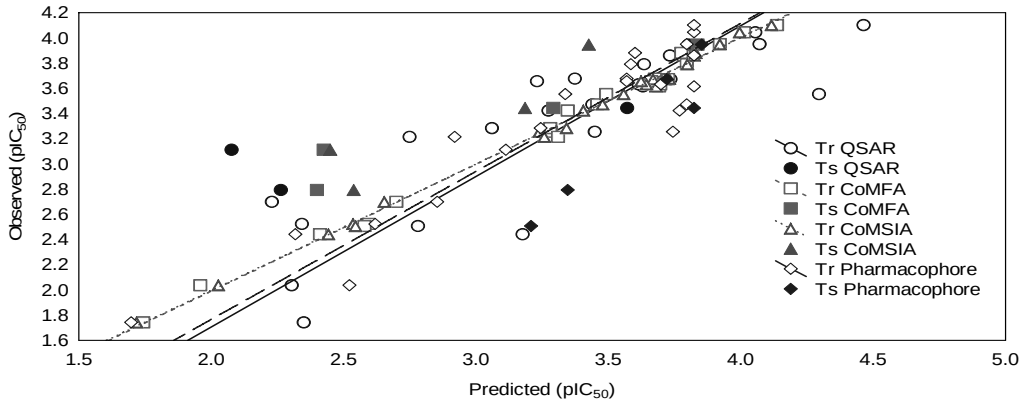

2D QSAR model, Tr: *n*=23, R^2=0.895, *se*=0.212, Q^2=0.726; Ts:*n*=4, R^2=0.780, *se*=0.282
CoMFA model, Tr: *n*=23, R^2=0.996, *se*=0.051, Q^2=0.841; Ts:*n*=4, R^2=0.936, *se*=0.166
CoMSIA model, Tr: *n*=23, R^2=0.997, *se*=0.040, Q^2=0.802; Ts: *n*=4, R^2=0.899, *se*=0.244
Pharmacophore model, Tr: *n*=22, Q^2=0.860, *rmsd*=1.344; Ts: *n*=5, R^2=0.912, *se*=0.205

Fig. 2: Observed vs predicted activity as per models.3D QSAR studies

Table 2: Results of CoMFA and CoMSIA studies

CoMFA	Components	n	R^2	se	F-value (df)	R^2_{cv}	sep	R^2_{bs}	sd	Contribution				
										s			e	
s	6	23	0.994	0.059	454.513 (6,16)	0.886	0.262	0.997	0.002	1.000				
e	6	23	0.985	0.093	180.697 (6,16)	0.479	0.542	0.986	0.007				1.000	
s+e	6	23	0.996	0.051	615.975 (6,16)	0.841	0.309	0.998	0.002	0.608			0.309	
CoMSIA	**Components**	**n**	**R^2**	**se**	**F-value (df)**	**R^2_{cv}**	**sep**	**R^2_{bs}**	**sd**	**Contribution**				
										a	**d**	**p**	**s**	**e**
a	2	23	0.713	0.415	6.635 (2,16)	0.446	0.516	0.787	0.079	1.000				
d	6	23	0.098	0.735	0.291 (6,16)	-	0.783	-	-		1.000			
p	6	23	0.991	0.072	306.392 (6,16)	0.791	0.354	0.996	0.002			1.000		
s	6	23	0.982	0.104	146.353 (6,16)	0.756	0.383	0.989	0.009				1.000	
e	6	23	0.978	0.115	118.629 (6,16)	0.627	0.459	0.996	0.003					1.000
s+e	6	23	0.995	0.054	552.063 (6,16)	0.822	0.327	0.997	0.003				0.405	0.595
s+e+a	6	23	0.994	0.059	457.482 (6,16)	0.818	0.331	0.997	0.003	0.121			0.367	0.513
a+s+p	6	23	0.998	0.039	1065.060 (6,16)	0.828	0.321	0.991	0.003	0.164		0.543	0.293	
s+e+p	6	23	0.995	0.056	504.250 (6,16)	0.797	0.349	0.998	0.001			0.381	0.243	0.376
a+p+s+e	6	23	0.997	0.040	982.290 (6,16)	0.802	0.344	0.999	0.001	0.109		0.336	0.218	0.337

s = Steric, e = Electrostatic, AlogP = Hydrophobicity, S_{18}=E-state indices at O_{18}, a=acceptor, d=donor, p=hydrophobicity

n=number of compounds in set, R^2 = Non-cross validated R^2, *se* = Standard error of estimate, R^2_{cv} = Cross-validated R^2 by LOO method, *sep* = Standard error of prediction, R^2_{bs} = Bootstrap R^2, sd = standard deviation

The best models for CoMFA and CoMSIA studies are characterized on the basis of maximum R^2_{cv}, *F*-value and R^2_{bs} (Table 2). The best CoMFA model (Fig 3) is obtained with 's' and 'e' fields exhibiting 60.8% and 39.2% contributions for the activity respectively. The model generated R^2 of 0.996 with *se* of 0.051, Q^2 of 0.841 with 6 components and standard error of prediction of 0.309, *F*-value of 615.975 and R^2_{bs} (bootstrap) is 0.998. The model also showed good predictivity (R^2_{pred}=0.936) for Ts set compounds. The predicted activity of the model is described in Fig 2 and mapped features are illustrated in Fig 3.

The contour maps of CoMFA model depicted green (steric favorable) and blue (electrostatic favorable) colors at 80% level of contribution, while yellow (steric unfavorable) and red colors (electrostatic unfavorable) show 20% level of contribution. The green contour suggests that presence of bulky substituents in the region favor activity, whereas presence of bulky substituent exhibiting steric influence in the yellow region is unfavorable for activity. Blue and red contours suggest the presence of positive charged substituents and negative charged groups favor the activity respectively. The model indicates that substitutional pattern at O_{18} (Fig 1) that imparts steric influence on that atom (O_{18}) is favorable, though steric influence in the vicinity of that substituent is unfavorable for the activity. Negative charge field at O_{18} and positive charge fields in the vicinity of atoms C_{13} and C_{14} are favorable for activity. Further substitutional pattern at R_3 that provides more electrostatic force field increases activity, but other sub-substitutional pattern at R_3 is favored by negative charge fields. The steric influence is unfavorable near atoms C_8 and C_9 region.

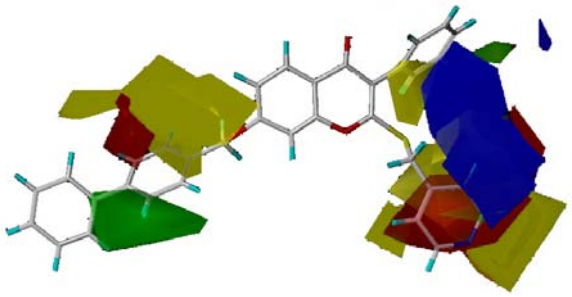

Fig. 3: Mapped features of most active compound (IC_{50}=0.079□M) in CoMFA model.

Steric: Green favorable, yellow unfavorable; Electrostatic: Blue favorable, red unfavorable

The best CoMSIA model (Fig 4) has been derived with 'a', 'p', 's' and 'e' fields that promote 10.9, 33.6, 21.8 and 33.7% contribution respectively to the activity. The regression coefficient (R^2) and error (*se*) of the model are 0.997 and 0.040 respectively, cross-validated coefficient (Q^2) of 0.802, error of prediction is 0.344 with 6 components, *F*-value of 982.290, R^2_{bs} is 0.999 with error of 0.001. The model further showed good predictivity (R^2_{pred}=0.899) for Ts set compounds. The contour maps are illustrated in Fig 4 and predicted activity is delineated in Fig 2.

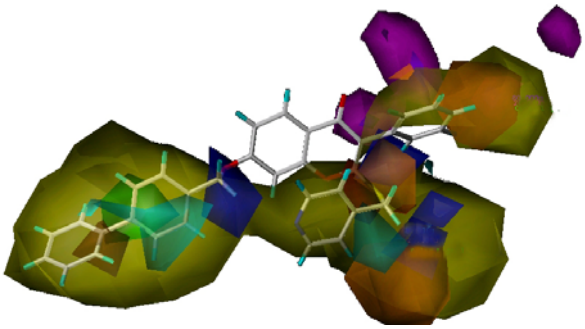

Fig. 4: Mapped features of most active compound in CoMSIA model.

Acceptor: Purple favorable, magenta unfavorable; Steric: Green favorable, yellow unfavorable; Hydrophobic: Cyan favorable, orange unfavorable; Electrostatic: Blue favorable, red unfavorable

The model indicates purple (80%, favorable) and magenta (20%, unfavorable) colors for acceptor (a) and reveals that R_1 and R_3 substituents are unfavorable as acceptors. Cyan (80%, favorable) and orange (20%, unfavorable) color contours represent hydrophobicity (p). Presence of substituents at O_{18} and C_8 can impart hydrophobicity of the molecule that favors activity, but sub-substitutional pattern on both those positions may unfavor for imparting hydrophobicity. Similarly substitutional pattern at R_1 is also unfavorable to impart hydrophobicity. For steric (s) and electrostatic (e) fields, similar results have been observed as with CoMFA model. The steric contours suggest that substitution at O_{18} that imparts steric property favors the activity, but other sub-substitutional pattern in molecular scaffold is unfavorable to impart steric property. The electrostatic contours indicate that positive charge substitutions at C_8 and C_{15} favor activity, whereas C_8 itself bearing negative charge is favorable for the activity. The model concludes that substitution at O_{18} that imparts steric property and behaves as hydrophobic region favor activity. Steric influence in regions of C_8 and C_9 is unfavorable for activity. C_8 itself imparts negative charge and substitutional pattern on that atom (C_8) brings hydrophobicity, both favor activity. Positive charge substitutions at position C_{14}, and at C_8 (R_3) and C_{15} (R_1) favor activity. Presence of HB acceptors at R_1 and R_3 shows negative influence on inhibitory activity.

Pharmacophore space modeling study

The result of the study is delineated in Table 3. The best hypothesis is characterized on the basis of highest cost difference (*Δcost*=105.597), root mean square deviation (*rmsd*=1.344), best correlation (Q^2=0.859) and test set prediction (R^2_{pred}=0.912). The mapped pharmacophore features of isoflavone derivative as CYP19 inhibitor are depicted in Fig 5. The best hypothesis demonstrated more than 92% correlation with the inhibitory activity to CYP19 and depicted that HB acceptor (a) and two hydrophobic (p) features might function as prime biophore for activity. The quality of the hypothesis is further adjudged through a cross-validation technique using Fischer's randomization test [22] at 99% confidence level and no other hypothesis generates better parameters than selected hypothesis. The predicted activities of the Tr and Ts sets are listed in Fig 2.

Table 3: Hypothesis parameters observed in Catalyst pharmacophore study

Run No.	Uncer-tainty	Weight variance	Spacing (pm)	Config.	Pharmacophore features in generated hypothesis	Cost				Q^2	rmsd
						Null	Fixed	Total	Δcost		
1	2	0.302	300	18.164	a, p, p	112.736	83.155	90.138	22.598	0.859	0.791
2	2	2	300	18.164	a, p, r	112.736	84.101	93.666	19.070	0.805	0.929
3	2	0.302	400	18.610	a, p, p	112.736	83.605	90.264	22.472	0.874	0.748
4	2	2	400	18.610	p, p, r, r	112.736	84.551	90.098	22.638	0.885	0.709
5	2	0.302	200	17.131	a, p, p	112.736	82.123	89.173	23.563	0.867	0.772
6	2	2	200	17.131	a, p, p, r	112.736	83.068	92.694	20.042	0.803	0.935
7	1.5	0.302	300	18.260	a, p, p	194.888	71.456	90.859	104.029	0.870	1.294
8	1.5	2	300	18.260	a, p, r	194.888	72.401	93.409	101.479	0.852	1.381
9	1.5	0.302	400	18.709	a, p, r	194.888	71.904	93.973	100.915	0.880	1.263
10	1.5	2	400	18.709	a, p, p	194.888	72.850	91.668	103.220	0.867	1.307
11	1.5	0.302	200	17.297	p, r, r, r	194.888	70.493	90.382	104.506	0.867	1.313
12	1.5	2	200	17.297	a, p, p	194.888	71.438	91.218	103.670	0.861	1.340
13	1.5	0.302	500	15.987	a, p, p	194.888	69.183	89.291	105.597	0.859	1.344

Input features: a, p, r; *a*: HB acceptor, *p*: Hydrophobic, *r*: Ring aromatic, *Δcost* = Null cost – total cost; *rmsd* = rms deviation; *n* = 22.

The mapped pharmacophore indicates that functional heteroatom, O_{11} behaves as promising HB acceptor that probably binds with the receptor by hydrogen bond. Presence of hydrophobic zones around atoms O_{18} and C_8 bring the compound more active, which can be adjudged with the observation of CoMSIA study. The critical inter-feature distances in 3D space of molecule impart selective CYP19 aromatase inhibition.

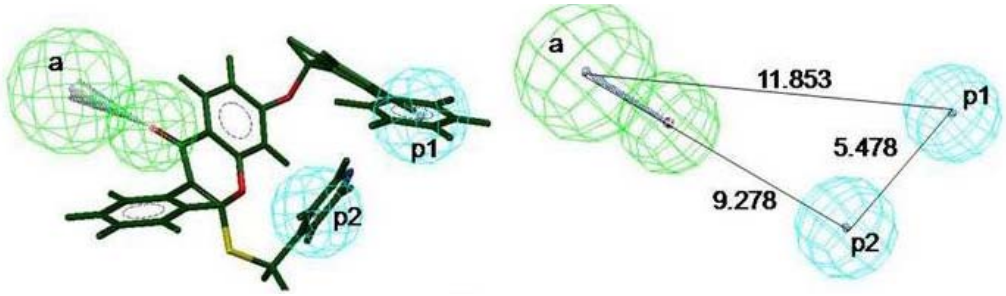

Fig. 5: Mapped features of most active compound in the pharmacophore model.

a: acceptor (green) and p: hydrophobic (sky blue)

CONCLUSION

In the present study, 2D/3D QSAR modeling and pharmacophore mapping studies have been performed for isoflavone molecular scaffold, identifying descriptors that contribute to biological activity, and search for pharmacophore elements responsible for inhibitory activity. The studies indicated that high electron density at O_{18} that imparts steric property and presence of substituent brings hydrophobicity of the molecule favor activity. Positive charge field with low electron density at C_{14} also favor activity. Steric influences in regions of C_8 and C_9 are unfavorable for activity. Positive charge substitutions at R_1 and R_3 favor activity. Negatively charged substitution at C_8 (R_3), which also shows hydrophobicity, favors activity. But presence of HB acceptors at R_1 and R_3 show negative influence on inhibitory activity. Keto functional groups (O_{11} and O_{18}) behave as promising HB acceptors that might interact with receptor residue. Ionization potential and molar refractivity also contribute for promoting activity.

ACKNOWLEDGEMENT

Financial support from Department of Science & Technology (FAST track award), Govt. of India is thankfully acknowledged. One of the authors S. Nagar thanks Council for Scientific and Industrial Research (CSIR), New Delhi for providing Senior Research Fellowship.

REFERENCES

1. Jemal A, Siegel R, Ward E, Hao Y, Xu J, Thun MJ. Cancer statistics, 2009. CA Cancer J Clin 2009; 59: 225–249.
2. Labrie F. Intracrinology. Mol Cell Endocrinol 1991; 78: C113–C118.
3. Cuzick J, Wang DY, Bulbrook RD. The prevention of breast cancer. Lancet 1986; 8472: 83–86.
4. Brueggemeier RW. Aromatase inhibitors in breast cancer therapy. Exp Rev Anticancer Ther 2002; 2: 181–191.
5. Meunier B, de Visser SP, Shaik S. Mechanism of oxidation reactions catalyzed by cytochrome P450 enzymes. Chem Rev 2004; 104: 3947–3980.
6. Thompson Jr EA, Siiteri PK. The involvement of human placental microsomal cytochrome P-450 in aromatization. J Biol Chem 1974; 249: 5373–5378.
7. Kellis Jr. JT, Vickery LE. Purification and characterization of human placental aromatase cytochrome P-450. J Biol Chem 1987; 262: 4413–4420.
8. Yoshida N, Osawa Y. Purification of human placental aromatase cytochrome P-450 with monoclonal antibody and its characterization. Biochem 1991; 30: 3003–3010.
9. Miller WR. Aromatase inhibitors: Mechanism of action and role in the treatment of breast cancer. Semin Oncol 2003; 30: 3–11.
10. Miller WR. Background and development of aromatase inhibitor. In: Furr BJA, editor. Aromatase inhibitors. Switzerland: Birkhauser Verlag; 2006. p. 1–21.
11. Nagy PI, Tokarski J, Hopfinger AJ. Molecular shape and QSAR analyses of a family of substituted dichlorodiphenyl aromatase inhibitors. J Chem Inf Comput Sci 1994; 34: 1190–1197.
12. Recanatini M. Comparative molecular field analysis of non-steroidal aromatase inhibitors related to fadrozole. J Comput Aided Mol Des 1996; 10: 74–82.

13. Nagar S, Islam A, Das S, Mukherjee A, Saha A. Pharmacophore mapping of flavones as potent aromatase inhibitor. Mol Diversity 2008; 12: 65–76.
14. Nagar S, Islam A, Das S, Mukherjee A, Saha A. Pharmacophore searching of benzofuran derivatives for selective CYP19 aromatase inhibition. Lett Drug Des Discov 2009; 6: 38–45.
15. Su B, Hackett JC, Dı´az-Cruz ES, Kim YW, Brueggemeier RW. Lead optimization of 7-benzyloxy 2-(40-pyridylmethyl)thio isoflavone aromatase inhibitors. Bioorg Med Chem 2005; 23: 6571–6577. b) Hackett JC, Kim YW, Su B, Brueggemeier RW. Synthesis and characterization of azole isoflavone inhibitors of aromatase. Bioorg Med Chem 2005; 12: 4063–4070. c) Kim YW, Hackett JC, Brueggemeier RW. Synthesis and aromatase inhibitory activity of novel pyridine-containing isoflavones. J Med Chem 2004; 16: 4032–4040.
16. Cramer III RD, Patterson DE, Bunce JD. Comparative molecular field analysis (CoMFA). 1. Effect of shape on binding of steroids to carrier proteins. J Am Chem Soc 1988; 110: 5959–5967.
17. Allen MS, Tan YC, Trudell ML, Narayanan K, Schindler LR, Martin MJ, Schultz C, Hagen TJ, Koehler KF. Synthetic and computer-assisted analyses of the pharmacophore for the benzodiazepine receptor inverse agonist site. J Med Chem 1990; 33: 2343–2357.
18. Klebe G, Abraham U, Mietzner T. Molecular similarity indices in a comparative analysis (CoMSIA) of drug molecules to correlate and predict their biological activity. J Med Chem 1994; 24: 4130–4146.
19. Böhm M, Stürzebecher J, Klebe G. 3D QSAR analyses using CoMFA and CoMSIA to elucidate selectivity differences of inhibitors binding to trypsin, thrombin and factor Xa. J Med Chem 1999; 42: 458 – 477.
20. Hoskuldsson A. PLS regression methods. J Chemometrics 1987; 2: 211–228.
21. Guner OF. Pharmacophore perception, development, and use in drug design. California: International University Line; 2002.
22. Snedecor GW, Cochran WG. Statistical methods. New Delhi: Oxford and IBH; 1967. p. 381–418.
23. Yang GF, Huang X. Development of quantitative structure-activity relationships and its application in rational drug design. Curr Pharm Des 2006; 12: 4601–4611.
24. CS Chem3D Pro and CS MOPAC Pro 5.0, Cambridge Soft, Cambridge, 2000. www.camsoft.com
25. Kier LB, Hall LH. An electrotopological-state index for atoms in molecules. Pharm Res 1990; 7: 801–807.
26. ETSA-CA, Chemical Technology, Calcutta University, Kolkata; 2007
27. CAChe 6.1, Computer-aided chemistry for macintosh and windows, Fujitsu Systems Business of America Inc. Chiba; 2000. www.CACheSoftware.com
28. TSAR 3D 3.3, Oxford molecular limited, Accelrys, San Diego; 2002. www.accelrys.com
29. Statistica 7.1, StatSoft Inc. Tulsa; 2005. www.statsoft.com
30. Wold S, Eriksson L. Chemometric methods in molecular design. In: de Waterbeemd HV, editor. Chemometric methods. Vol. 2. Weinheim; VCH Verlagsgesellschaft mbh; 1995. p. 312.
31. Cramer III RD, DePriest SA, Patterson DE, Hecht PE. The developing practice of comparative molecular field analysis. In: Kubinyi H, editor. 3D QSAR in drug design-theory, methods and applications. Leiden: ESCOM Science; 1993. p. 443–485.
32. Viswanadhan VN, Ghose AK, Revankar GR, Robins RK. Atomic physicochemical parameters for three dimensional structure directed quantitative structure-activity relationships. 4. Additional parameters of hydrophobic and dispersive interactions and their application for an automated superposition of certain naturally occurring nucleoside antibiotics. J Chem Inf Comput Sci 1989; 29: 163–172.
33. Kirkpatrick S, Gelatt CD, Vecchi Jr MP. Optimization by simulated annealing. Science 1983; 220: 671–680.
34. Purcel WP, Singer JA. A brief review and table of semiempirical parameters used in the Hückel molecular orbital method. J Chem Eng Data 1967; 12: 235–246.
35. Vinter JG, Davis A, Saunders MR. Strategic approaches to drug design. I. An integrated software framework for molecular modeling. J Comp Aided Mol Des 1987; 1: 31–51.
36. SYBYL 7.3, Tripos Inc, St. Louis; 2006. www.tripos.com
37. Catalyst 4.11, Accelrys Inc, San Diego, CA; 2005. www.accelrys.com
38. Schuster D, Laggner C, Steindl TM, Palusczak A, Hartmann RW, Langer T. Pharmacophore modeling and in silico screening for new P450 19 (aromatase) inhibitors. J Chem Inf Mod 2006; 3: 1301–1311.
39. Kier LB. Shape indexes of orders one and three from molecular graphs. Quant Struct -Act Relat 1986; 5: 1–7.
40. Karelson M, Lobanov VS. Quantum-chemical descriptors in QSAR/QSPR studies. Chem Rev 1996; 96: 1027–1043.
41. Ghosh AK, Crippen GM. Atomic physicochemical parameters for three-dimensional-structure-directed quantitative structure-activity relationships. 2. Modeling dispersive and hydrophobic interactions. J Chem Inf Comput Sci 1987; 27: 21–35.